



Progression of Atrophy and Visual Outcomes in Extensive Macular Atrophy with Pseudodrusen-like Appearance

Francesco Romano, MD,¹ Matteo Airal di, MD,¹ Mariano Cozzi, MSc,¹ Marta Oldani, MD,¹ Ester Riva, MSc,¹ Alice Ingrid Bertoni, BSc,¹ Astrit Dautaj, MD,² Matteo Bertelli, MD,³ Giovanni Staurenghi, MD,¹ Anna Paola Salvetti, MD¹

Purpose: To report visual outcomes and rate of retinal pigment epithelium (RPE) atrophy progression in patients with extensive macular atrophy with pseudodrusen-like appearance (EMAP).

Design: Retrospective, observational study.

Participants: Patients with EMAP and symptom onset before 55 years of age, at least 12 months of follow-up using Spectralis blue-light fundus autofluorescence (BAF) and OCT and with no other ocular or systemic conditions.

Methods: Best-corrected visual acuity (BCVA), BAF, and OCT images were reviewed at baseline and at each annual visit until the last available follow-up. Atrophy was measured by 2 graders using the region finder software on Heidelberg Explorer and confirmed using OCT scans covering the entire atrophic lesion. The following imaging biomarkers were analyzed at each visit: foveal atrophy, vitreomacular traction, outer retinal tubulations, choroidal caverns and subfoveal choroidal thickness, border autofluorescence pattern (hyper-autofluorescent or iso-autofluorescent), and border irregularity as expressed by circularity index (CI).

Main Outcome Measures: Primary outcomes were annual rate of atrophy enlargement and BCVA loss in EMAP patients. Secondary outcomes included the assessment of potential factors able to predict disease progression.

Results: Thirty-six eyes from 18 patients with EMAP (6 men [33%]; mean age at symptom onset, 48.1 ± 1.7 years) were included. Mean follow-up lasted 32.8 ± 14.3 months. RPE atrophy increased from 10.8 ± 6.3 mm² at baseline to 18.1 ± 8.3 mm² at the end of follow-up, with a rate of 2.91 ± 1.09 mm²/year. Faster progression was associated with smaller CI at baseline ($P = 0.02$) and with iso-autofluorescent lesion borders ($P = 0.01$). Visual acuity declined progressively at a rate of 7.4 ± 5.8 letters per year, with 57% of eyes showing vision of 20/200 Snellen or worse at the 4-year follow-up. Worse visual outcomes were observed in patients with early foveal involvement at baseline ($P = 0.02$).

Conclusions: Patients affected by EMAP present a rapid expansion of RPE atrophy that is comparable with the diffuse-trickling form of geographic atrophy. More irregular and iso-autofluorescent lesion borders seem to predict faster progression. Our findings may provide relevant information for patient counseling and future interventional approaches to select the best candidates and proper clinical outcomes. *Ophthalmology Science* 2021;1:100016 © 2021 Published by Elsevier Inc. on behalf of the American Academy of Ophthalmology. This is an open access article under the CC BY-NC-ND license (<http://creativecommons.org/licenses/by-nc-nd/4.0/>).



Supplemental material available at www.ophtalmologyscience.org/.

Extensive macular atrophy with pseudodrusen-like appearance (EMAP) is a rare form of macular degeneration characterized by bilateral atrophic lesions with a larger vertical axis.¹ The macular atrophy typically is surrounded by diffuse pseudodrusen-like deposits extending into the midperiphery, and paving stone lesions are frequently located in the far retinal periphery.¹

Clear genetic or pathogenic features behind this condition have not been defined so far; however, a possible toxic mechanism resulting from long-term or low-dose exposure

to pesticides has been hypothesized because of a higher disease incidence observed in French regions with significant industrial and farming activities.² Although some clinical and imaging features resemble those of age-related macular degeneration (AMD), EMAP affects younger people, mainly women, who initially report night blindness followed by a rapid, progressive decline in central vision.^{1,3}

Blue-light fundus autofluorescence (BAF) is a fast and reliable imaging method that is used commonly to assess the presence and the progression of macular atrophy in different

retinal disorders.^{4–8} The loss of lipofuscin or melanolipofuscin after atrophy of the retinal pigment epithelium (RPE) cells generates a marked reduction of the autofluorescence signal that can be measured easily by a variety of postprocessing tools.^{5,9,10}

Although the rapid disease progression occurring in EMAP already has been described in the literature, no study to date has reported the rate of RPE atrophy enlargement and the possible factors influencing the course of the disease.^{1,3,11–13} The aim of this study was to assess the annual rate of atrophy expansion in EMAP patients using BAF and possibly to identify demographic, clinical, and imaging features predictive of faster disease progression and worse visual outcomes.

Methods

This study was designed as a retrospective, observational, single-center investigation. Medical records and imaging studies of patients with EMAP seeking treatment at the Eye Clinic of Luigi Sacco Hospital, Milan, Italy, from December 2014 through February 2019 were reviewed systematically. The research followed the tenets of the Declaration of Helsinki and was approved by the local institutional review board. All study participants provided written informed consent.

Study Participants

Patients had to fulfill the following criteria to be included in the study: (1) diagnosis of EMAP defined as the presence of macular atrophy with larger vertical axis surrounded by widespread pseudodrusen-like deposits; (2) age younger than 55 years at diagnosis or at onset of visual symptoms, including nyctalopia, reduced vision, and metamorphopsias; (3) a minimum of 12 months of follow-up with Spectralis BAF images and OCT (Heidelberg Engineering) scans encompassing the entire area of RPE atrophy at the posterior pole; and (4) acceptable fixation. Exclusion criteria were: (1) any systemic or ocular condition known to cause similar retinal alterations or potentially affecting our analysis; (2) the development of macular neovascularization; (3) the detection of disease-causing genetic mutations associated with macular or retinal dystrophies, or both; (4) positive family history for inherited retinal dystrophies; (5) any ocular surgery in the previous 12 months; and (6) significant media opacities leading to poor image quality.

Study Protocol

Clinical records were reviewed with particular interest in age at diagnosis, age at symptom onset, gender, best-corrected visual acuity (BCVA), detailed family history with regard to ocular diseases and visual symptoms, duration of follow-up, and previous ocular treatments.

All EMAP patients underwent a complete ophthalmic examination at baseline, including BCVA assessment using Early Treatment Diabetic Retinopathy Study (ETDRS) charts, slit-lamp biomicroscopy with funduscopy, Goldmann applanation tonometry, color fundus photography, BAF (488-nm excitation, 495-nm barrier filter) and OCT with a Spectralis HRA+OCT instrument, and fluorescein and indocyanine green angiography using a Spectralis HRA2 instrument.

Genetic testing for the 148 genes known to be the cause of nonsyndromic retinal dystrophies was performed using parallel mass sequencing of target regions with Nextera Rapid Capture

method on the Illumina MiSeq platform. Because no known gene has been linked to EMAP, the full panel of inherited retinal dystrophy genes were analyzed to exclude a new phenotype caused by a previously known gene (Supplemental Table 1).

Best-corrected visual acuity, BAF images, and OCT scans at baseline and at each annual visit until the last available follow-up were reviewed. Considering the retrospective design and real-life setting of our study, visits performed within 2 months from the scheduled time frame were accepted and included in our analysis.

Imaging Analysis

Retinal pigment epithelium atrophy was defined as sharp and demarcated areas of reduced autofluorescence signal at the posterior pole on BAF images (30° × 30° field of view) centered on the fovea. Quantification of atrophy was performed by 2 independent graders (M.C. and F.R.) who were unaware of the patients' clinical records using the Expert modus tool of the Heidelberg region finder software (version 2.6.4). The mean value between the 2 measurements was used for our analysis.

Because hypo-autofluorescent signal can be generated by retinal alterations other than RPE atrophy (e.g., drusen and pigmentary changes), the simultaneous consultation of OCT dense raster scans covering the entire area of atrophy (25° × 30°, 61 scans with at least 16 automatic real-time tracking frames per scan) was allowed to refine the delineation of atrophic borders.¹⁴ On the OCT scans, atrophy was defined, as recommended by the latest Classification of Atrophy Meeting Report,¹⁵ as a region of at least 250 μm in diameter characterized by attenuation of the RPE and of the overlying outer retinal layers and by thinning of the outer nuclear layer with consequent signal hypertransmission into the choroid.¹⁵ The methodology used to assess atrophy progression is shown in Figure 1.

Enlargement of RPE atrophy was defined as the expansion of pre-existing areas compared with baseline. The rate of progression was calculated by subtracting the change in size at each time point. Because atrophy may progress at a nonlinear rate, we performed the square root transformation of lesion areas as described already for AMD.¹⁶ A number of factors with potential prognostic value for an individual rate of progression of the RPE atrophy were investigated thoroughly at each examination by the same graders.¹⁶ In case of significant discordance between the 2 readers, a third grader (A.P.S.) was consulted.

OCT scans were inspected for the presence of fovea involvement by atrophy; vitreomacular traction; outer retinal tubulations, that is, branching tubular structures in the outer nuclear layer on en face OCT scans appearing as circles on cross-section¹⁷; choroidal caverns, that is, hyporeflective, round cavities variably localized in the Sattler and Haller's layers¹⁸; and measurement of subfoveal choroidal thickness from the outer margin of the hyperreflective RPE to the hyporeflective margin corresponding to the sclerochoroidal interface.¹⁹

Normalized BAF images were reviewed to assess the BAF patterns of the lesion borders (hyper-autofluorescent or iso-autofluorescent) and the lesion configuration expressed by the circularity index (CI). In detail, CI is an index proposed to evaluate the deviation of the atrophic lesion perimeter from a perfect circle.²⁰ For this analysis, BAF pictures were exported from Heidelberg Eye Explorer software (version 1.10.4.0) as .tiff files and loaded into ImageJ software (National Institutes of Health). Calibration of the image scale on ImageJ was achieved matching the metric (millimeters) and pixel dimensions of each BAF image, as provided by the Heidelberg Eye Explorer software. The perimeter of the EMAP-related atrophy then was outlined manually, and the area expected for that given perimeter was measured as described in the literature.²⁰ The CI was calculated as

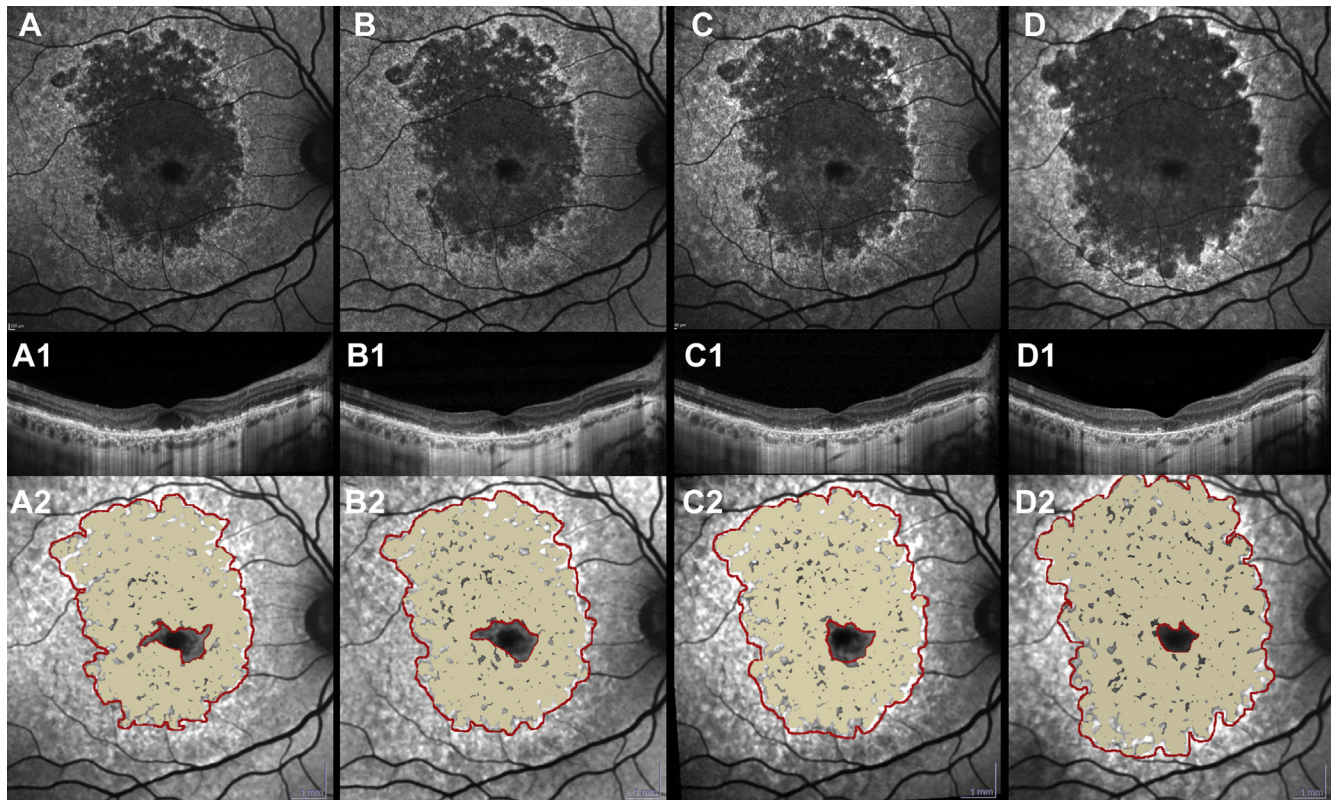


Figure 1. Measurement of macular atrophy (MA) in a patient affected by extensive macular atrophy with pseudodrusen-like appearance from baseline (A–A2) to the last available follow-up at 36 months (D–D2). A–D, The first row shows the annual progression of MA using blue-light fundus autofluorescence, whereas the second row (A1–D1) displays the corresponding OCT passing through the fovea. Of note, the pseudodrusen-like material lying above the Bruch’s membrane disappeared progressively with follow-up, leaving space for MA characterized by thinning of outer retinal layers and choroidal signal hypertransmission. The use of the expert modus of Region Finder software (Heidelberg Engineering) is depicted in the bottom row (A2–D2); the measured area is yellow, whereas constraints are outlined in red. In this specific patient, visual acuity dropped from 20/50 to 20/320 Snellen equivalent.

the ratio between the actual atrophic area measured using the Heidelberg Eye Explorer and the expected area relative to the measured perimeter, with values closer to 0 indicating more irregular shapes and values closer to 1 indicating more circular shapes. All the investigated imaging prognostic factors are depicted in [Figure 2](#).

Study Outcomes

The primary outcome of our study was to report the annual rate of RPE atrophy enlargement in patients affected by EMAP. Secondary outcomes included the assessment of potential clinical and imaging biomarkers associated with faster atrophy progression and worse visual outcomes.

Statistical Analysis

All statistical analyses were performed using RStudio version 1.3.959 (PBC) with significance set at $P < 0.05$. Descriptive statistics were presented as mean \pm standard deviation (range) or as frequency (percentage) where appropriate.

The following variables were analyzed at baseline, at 12 months, and when available, at 24, 36, and 48 months: age, gender, eye laterality, BCVA, area of RPE atrophy, progression rate of atrophy (before and after square root transformation), fovea involvement, vitreomacular traction, the presence of outer retinal tubulations and of choroidal caverns, subfoveal choroidal

thickness, BAF pattern of atrophy borders (hyper-autofluorescent or iso-autofluorescent), and CI.

Normal distribution of our cohort was assessed using the Shapiro-Wilk test. Student’s t test for dependent and independent measurements was used to assess intraindividual and interindividual differences, whereas Pearson’s correlation test was used to explore the possible correlations among variables.

The prognostic factors then were analyzed using a multivariate analysis; this approach was used to investigate the effect of such variables on the rate of RPE atrophy progression and on visual outcomes. After nesting for patient identity, eye laterality, and time, all the prognostic factors were investigated further using linear mixed-effect models as fixed effects in the attempt to establish a predictive model for the rate of atrophy progression and for visual function.

Interobserver agreement for the 2 independent graders (F.R. and M.C.) was tested using intraclass correlation coefficients (with 95% confidence intervals) and Cohen’s κ statistics (with 95% confidence intervals) for quantitative and qualitative variables, respectively.

Results

A total of 18 EMAP patients (36 eyes) were included in our study, with 6 men (33.3%) and 12 women (66.7%). One



Figure 2. Imaging features investigated for possible association with faster disease progression. The blue-light fundus autofluorescence characteristics analyzed are shown in the left column, whereas OCT findings are presented in the right column.

patient was excluded because of development of bilateral macular neovascularization during follow-up. The mean age of our cohort at baseline examination was 55.3 ± 2.7 years (range, 50–60 years), whereas the mean age at symptoms onset was of 48.1 ± 1.7 years (range,

44–51 years). Macular atrophy with a predominant vertical axis and diffuse pseudodrusen-like deposits extending to the mid-peripheral retina were present in all patients at baseline, whereas peripheral paving-stone degeneration was documented in 29 eyes (80.6%). Hard

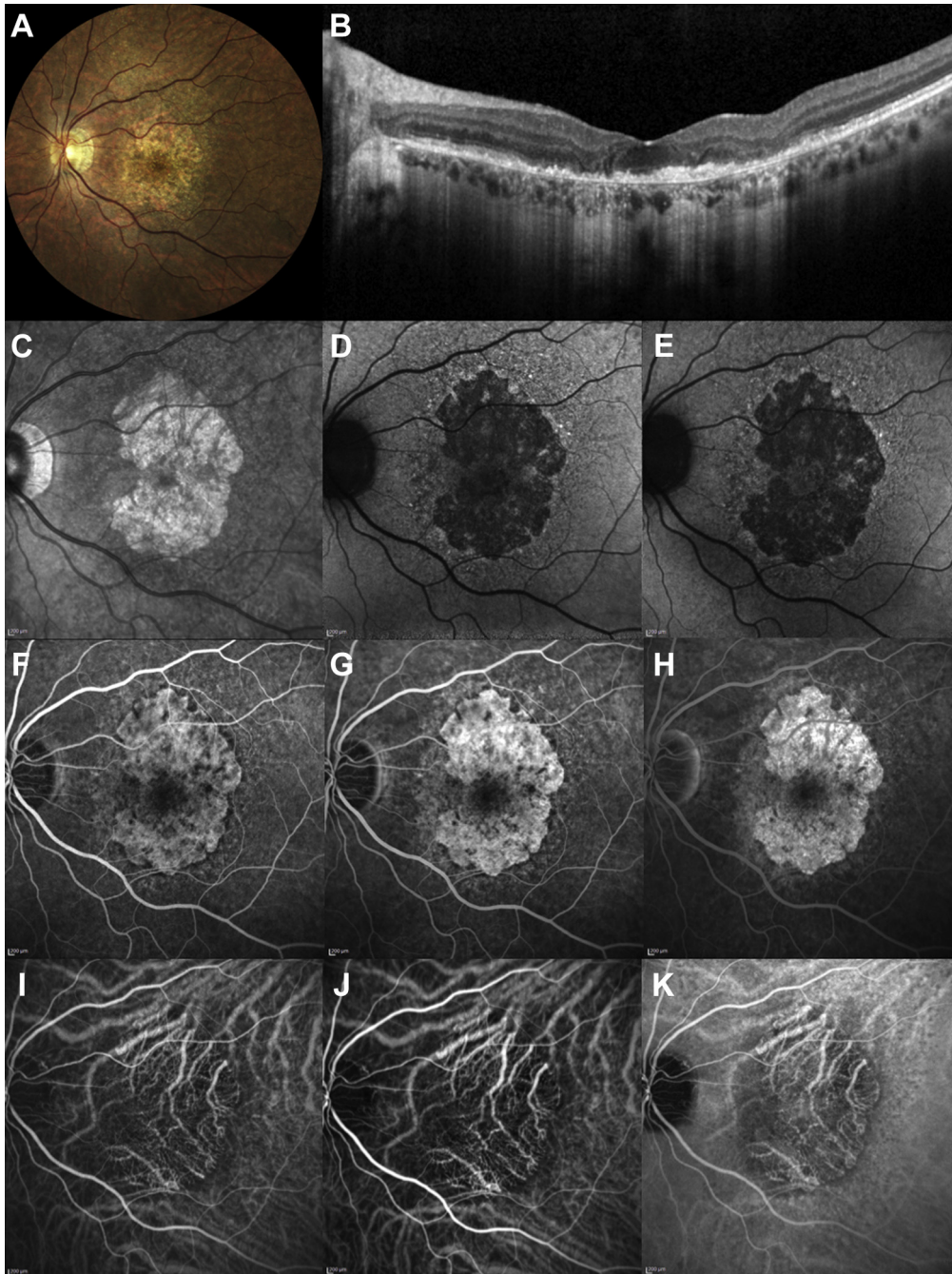


Figure 3. A representative case of extensive macular atrophy with pseudodrusen-like appearance using multimodal imaging. **A**, Color fundus photography showing a large macular atrophic area with a predominant vertical axis surrounded by pseudodrusen-like deposits. **B**, OCT scan showing collapse of the perifoveal outer retinal layers with choroidal hypertransmission, whereas the fovea appears unaffected, as evidenced by the preserved central vision (20/32 Snellen). **C–E**, The extension of the atrophic lesion can be appreciated on **(C)** near-infrared reflectance, **(D)** blue-light fundus autofluorescence, and **(E)** green autofluorescence. **F–K**, The corresponding **(F–H)** fluorescein angiography and **(I–K)** indocyanine green angiography appearance of extensive macular atrophy with pseudodrusen is depicted at 40 seconds and 3 and 10 minutes.

and soft drusen typical of AMD were not identified in any of the patients. A representative case of EMAP is illustrated in [Figure 3](#).

Results of genetic testing using a targeted next-generation sequencing panel for nonsyndromic retinal dystrophies did not explain the retinal disease in any patient, but

revealed variants of unknown significance in 5 patients (27.8%; see [Supplemental Fig 1](#)).

The mean follow-up period lasted 32.8 ± 14.3 months (range, 12–49 months), with 26 eyes having at least 2 years of follow-up and 14 eyes having 4 years of follow-up. Complete demographic and clinical characteristics are

Table 1. Demographic and Clinical Features of the Studied Cohort

Feature	Data
No. of patients (eyes)	18 (36)
Age at baseline (yrs)	
Mean \pm SD	55.3 \pm 2.7
Range	50–60
Age at symptom onset	
Mean \pm SD	48.1 \pm 1.7
Range	44–51
Gender, no. (%)	
Male	6 (33.3)
Female	12 (66.7)
Eye laterality, no. (%)	
Right	18 (50)
Left	18 (50)
Length of follow-up (mos)	
Mean \pm SD	32.8 \pm 14.3
Range	12–49
Annual atrophy progression rate (mm ² /yr), mean \pm SD	2.91 \pm 1.09
Annual BCVA loss (ETDRS letters/yr), mean \pm SD	7.4 \pm 5.8

BCVA = best-corrected visual acuity; ETDRS = early treatment diabetic retinopathy study; SD = standard deviation.

reported in Table 1. Agreement between the 2 graders was considered acceptable for both quantitative (intraclass correlation coefficient, 0.866; 95% confidence interval, 0.814–0.908) and qualitative ($\kappa = 0.89$; 95% confidence interval, 0.83–0.94) measurements.

Baseline Imaging Features

At baseline BAF assessment, all eyes showed signs of RPE atrophy at the posterior pole (range, 1.03–27.01 mm²). Twenty-six eyes (72.2%) demonstrated hyper-autofluorescent borders, whereas 12 of them showed iso-autofluorescent borders (27.8%) compared with background. The CI of the cohort increased progressively from 0.26 \pm 0.19 at baseline to 0.36 \pm 0.17 at the last follow-up visit ($P < 0.001$).

Baseline OCT examination revealed the presence of outer retinal tubulations in 5 eyes (13.9%) and of choroidal caverns in 7 eyes (19.4%). Foveal involvement by RPE

atrophy was identified in 13 eyes (36.1%) at presentation, whereas subfoveal choroidal thickness already was reduced markedly (136 \pm 60 μ m) and thinned out progressively during the follow-up (last visit, 110 \pm 58 μ m; $P < 0.001$). Complete imaging data at baseline and follow-up are listed in Table 2.

Assessment of Atrophy Progression

The mean area of RPE atrophy at baseline was 10.8 \pm 6.3 mm² and reached 18.1 \pm 8.3 mm² at the end of follow-up ($P < 0.001$). The annual rate of atrophy progression was 2.91 \pm 1.09 mm²/year. The rate of progression negatively and significantly correlated with baseline CI ($r = -0.631$; $P < 0.001$) and was higher in eyes showing foveal atrophy at baseline ($t = 2.18$; $P = 0.04$).

When assessed using multivariate analysis ($R^2 = 0.662$; $P < 0.001$), the progression rate of atrophy was found to be affected significantly by a smaller CI at baseline ($P = 0.005$), the presence of iso-autofluorescent borders ($P = 0.01$), and a smaller atrophic area at baseline ($P = 0.007$; Supplemental Table 2).

After applying the square root transformation, the resulting progression rate was greater in eyes with iso-autofluorescent borders of RPE atrophy ($t = 2.85$; $P = 0.007$). Multivariate analysis ($R^2 = 0.650$; $P < 0.001$) revealed that faster expansion of atrophy was associated with a smaller CI at baseline ($P = 0.017$), iso-autofluorescent borders of atrophy ($P = 0.01$), and the identification of choroidal caverns on OCT ($P = 0.04$, Supplemental Table 2).

Fixed effects (prognostic factors) and random effects (patient-specific and time) mixed models were able to explain 97% to 98% of the progression rate for our data (conditional $R^2 = 0.97$; $R^2 = 0.98$ after square root transformation), and this was attributable principally to the fixed effects (marginal $R^2 = 0.94$ for both analyses, where conditional R^2 refers to the model as a whole and marginal R^2 accounts for the fixed effects only).

Assessment of Visual Function

The mean BCVA at baseline was 67.1 \pm 15.8 ETDRS letters (range, 40–84 letters) and dropped significantly to

Table 2. Main Imaging Characteristics at Baseline and at Last Follow-up Visit

Characteristic	Baseline	Last Follow-up	P Value
Area of RPE atrophy (mm ²), mean \pm SD	10.8 \pm 6.3	18.1 \pm 8.3	<0.001
BCVA (ETDRS letters), mean \pm SD	67.1 \pm 15.8	49.8 \pm 21.2	<0.001
Circularity index, mean \pm SD	0.26 \pm 0.19	0.36 \pm 0.17	<0.001
Hyper-autofluorescent edges, no. (%)	26 (72.2)	27 (75.0)	<0.001
Fovea involvement, no. (%)	13 (36.1)	30 (83.3)	<0.001
Vitreomacular traction, no. (%)	0 (0)	4 (11.1)	0.11
Outer retinal tubulations, no. (%)	5 (13.9)	14 (38.9)	<0.001
Choroidal caverns, no. (%)	7 (19.4)	17 (47.2)	0.01
Choroidal thickness (μ m), mean \pm SD	136 \pm 60	110 \pm 58	<0.001

BCVA = best-corrected visual acuity; ETDRS = Early Treatment Diabetic Retinopathy Study; RPE = retinal pigment epithelium; SD = standard deviation.

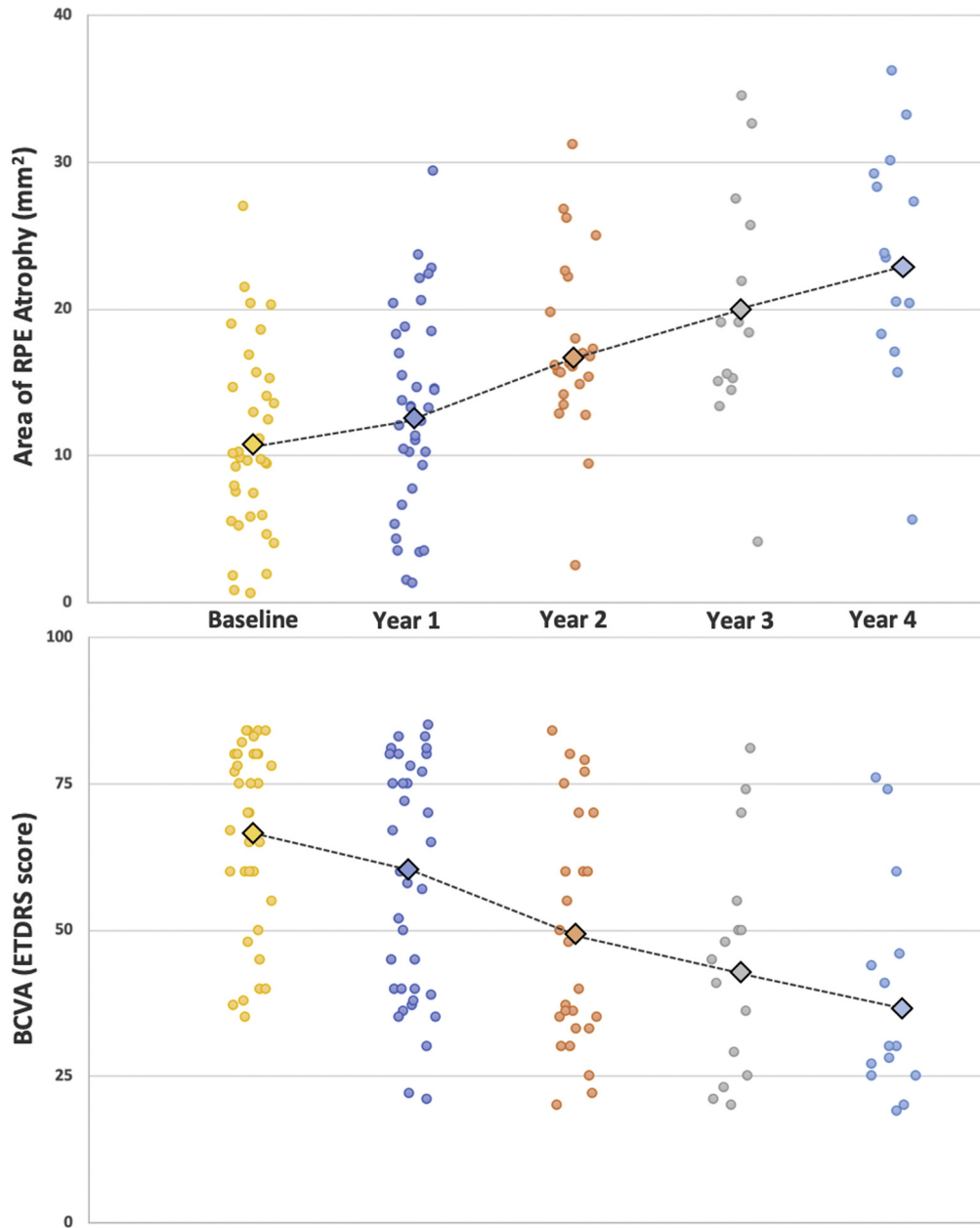


Figure 4. Scatterplot showing retinal pigment epithelium (RPE) atrophy progression and visual acuity variation. The visual loss mirrors the enlargement of RPE atrophy during the entire follow-up. BCVA = best-corrected visual acuity; ETDRS = Early Treatment Diabetic Retinopathy Study.

49.8 ± 21.2 ETDRS letters at the end of follow-up ($P < 0.001$). The annual rate of BCVA loss corresponded to 7.4 ± 5.8 letters. Overall, 58% of study eyes lost 3 or more ETDRS lines at 2 years, whereas 64% of eyes lost 3 or more lines at 4 years. Thirty-eight percent of eyes showed a BCVA of 35 ETDRS letters or worse at 2 years (Snellen equivalent, approximately 20/200) and 57% of eyes did so at 4 years. Worse final visual acuity was associated at any time point with larger size of RPE atrophy ($r = -0.646$; $P < 0.001$), thinner subfoveal choroidal thickness ($r = 0.405$; $P = 0.03$), and foveal involvement by atrophy ($t = 3.33$; $P = 0.008$). On multivariate analysis, the rate of BCVA loss was affected positively and meaningfully only by the early detection of

foveal atrophy at baseline ($P = 0.016$; $R^2 = 0.622$; $P < 0.001$; [Supplemental Table 3](#)). Fixed effects were able to predict only 54% of our model of BCVA decline (marginal $R^2 = 0.54$), reaching 83% when nesting for time and eye laterality of each patient (conditional $R^2 = 0.83$). Changes in atrophy size and visual acuity during the follow-up are plotted in [Figure 4](#).

Discussion

This study analyzed the enlargement of RPE atrophy in patients with EMAP using BAF and OCT. We found that

Table 3. Clinical Characteristics of Extensive Macular Atrophy with Pseudodrusen-like Appearance

Characteristic	Data
Age at symptom onset/ diagnosis	45–55 years
Gender	Female predominance
Size and shape of MA	Extensive, polycyclic and symmetric atrophic lesions with larger vertical axis
Progression rate of MA	$2.91 \pm 1.09 \text{ mm}^2/\text{year}$
BAF characteristics	Grayish atrophy at the posterior pole with either hypo-autofluorescent or iso-autofluorescent borders
OCT features	Significant thinning of ONL; loss of ELM, EZ, and RPE; RPE–Bruch's membrane splitting with RPD-like deposits; severe choroidal thinning
Foveal involvement	Relatively early
MNV development	Rare
Peripheral lesions	Frequent pseudodrusen-like deposits until mid periphery; peripheral paving stone lesions

BAF = blue-light fundus autofluorescence; ELM = external limiting membrane; EZ = ellipsoid zone; MA = macular atrophy; MNV = macular neovascularization; ONL = outer nuclear layer; RPD = reticular pseudodrusen; RPE = retinal pigment epithelium.

the annual rate of atrophy expansion approached $3 \text{ mm}^2/\text{year}$, leading to foveal involvement in 83% of eyes at the end of follow-up. Moreover, patients with EMAP experienced severe visual loss during the follow-up (7 ETDRS letters/year), particularly when foveal atrophy was detected early during the course of the disease.

In middle-aged individuals, EMAP is a well-established cause of severe macular atrophy characterized by fast progression, a more pronounced vertical axis, and early foveal involvement.^{1–3} To date, the fast progression of RPE atrophy has been ascribed principally to the presence of confluent pseudodrusen-like deposits as already occur in some forms of AMD.^{3,21,22} However, no quantitative data are present in the literature regarding its rate of enlargement. We found that patients with EMAP demonstrate an annual progression rate that is greater than the one commonly observed in geographic atrophy secondary to AMD (range, $0.53\text{--}2.60 \text{ mm}^2/\text{year}$), with the exception of the diffuse-trickling geographic atrophy.^{4,23–25}

Interestingly, we noted several analogies between the diffuse-trickling phenotype of geographic atrophy and the patients with EMAP in this study using multimodal imaging, including the splitting between the RPE and the Bruch's membrane on OCT images, the grayish appearance of the atrophic lesions on autofluorescence, and the fast progression of macular atrophy with a major vertical orientation.²³ Based on our findings, we hypothesize that EMAP may be one of the possible underlying causes of the diffuse-trickling phenotype because of early retinal degeneration caused by currently unknown genetic and possible environmental factors.² In this view, further genetic and epidemiologic studies aimed at identifying novel predisposing elements will be critical to refining EMAP pathogenesis. Following

the work of Hamel et al¹ when EMAP was described initially, we suggest an updated table based on our observations summarizing the principal clinical and imaging elements present in EMAP (Table 3).

Similar rates of geographic atrophy growth have been observed in other retinal degenerative conditions, such as pseudoxanthoma elasticum and Sorsby fundus dystrophy, particularly in the absence of macular neovascularization.^{26,27} Because the exact cause behind EMAP remains elusive, involvement of a diseased Bruch's membrane in its pathogenesis is possible.

Because of the interpatient variability in the progression rate, we investigated some imaging prognostic factors in the attempt to predict lesions with faster atrophy enlargement and thus to provide patients with a more accurate prognosis. After applying the square root transformation to the observed progression rate to eliminate the dependency on the baseline area,^{21,28} our results showed that the detection of iso-autofluorescent and more irregular (lower CI) atrophy borders significantly affect the progression rate in EMAP. Although irregular configuration of the borders already has been linked to faster progression of atrophy in other retinal disorders because of the increased RPE perimeter at risk, the different autofluorescence patterns observed at junctional regions are more difficult to explain. Although the detection of hyper-autofluorescent borders originally was associated with fast-progressing forms of geographic atrophy, recent clinicopathologic studies demonstrated that the rim surrounding atrophic lesions is not related to the atrophy enlargement rate, but can be explained by stacked RPE cells, rather than lipofuscin accumulation.^{29–31} Based on our findings, we hypothesize that areas characterized by the coalescence of pseudodrusen-like deposits are the most likely and rapid to develop atrophy. The heterogeneous material content produces a mixed autofluorescence signal, potentially contributing to the iso-autofluorescent pattern seen in 28% of the eyes in this study. In addition, the high predictive value of the tested factors (marginal $R^2 = 0.94$) confirms the goodness of our model, suggesting that such parameters may turn out to be useful in future interventional approaches to select or stratify patients according to similar likelihood of progression.

Severe visual acuity loss is another relevant concern that mirrors the expansion of atrophy in patients with EMAP.³ Visual symptoms begin as difficulties with dark adaptation and rapidly progress to the development of central scotomas until legal blindness ensues.¹ We estimated that BCVA decline proceeds at a rate of 7 ETDRS letters per year starting from clinical diagnosis and particularly drops when signs of foveal atrophy are visible with OCT already at baseline examination. Unfortunately, the precise impact of macular atrophy on visual function during the course of the disease remains difficult to appraise because several pathologic alterations possibly precede the development of frank RPE and outer retinal atrophy.

Our correlation analysis also suggested that worse vision is influenced by thinner subfoveal choroidal thickness. This finding supports the fact that choroidal thinning frequently accompanies RPE atrophy, reticular pseudodrusen, and

basal laminar deposits.^{22,32} Finally, our model was able to predict 83% of BCVA changes and was especially affected by random effects such as time. These data emphasize that early and accurate diagnosis will become crucial in case of clinical trials that advance to select the correct timing for experimental treatments.

We acknowledge that our study has numerous limitations, especially if we consider its retrospective design and the small sample size of our cohort. Indeed, EMAP is a rare form of macular degeneration whose pathophysiologic features and diagnostic criteria remain ill-defined, thus making patient recruitment challenging. Moreover, the assessment of atrophic areas for the progression rate might have been influenced by the presence of pseudodrusen altering the BAF signal; however, the agreement between the 2 readers was high, thus ensuring the repeatability of

our measurements. Other potential limitations include the relatively short follow-up and the absence of functional data other than BCVA (e.g., microperimetry and multifocal electroretinography) and the lack of OCT angiography data as possible biomarkers of progression (e.g., vessel density and flow voids) and to assess the extension of atrophy.^{33–35}

In conclusion, our investigation explored the rate of RPE atrophy expansion and visual outcomes in patients affected by EMAP. The irregularity and the autofluorescent pattern of the lesion borders seem to be the major predictors of atrophy expansion, whereas visual acuity seems particularly affected by an early foveal involvement during the course of the disease. Our results may provide relevant information for future therapeutic strategies to identify the best candidates and to set proper clinical outcomes.

Footnotes and Disclosures

Originally received: March 7, 2021.

Final revision: March 15, 2021.

Accepted: March 15, 2021.

Available online: March 19, 2021.

Manuscript no. D-21-00036.

¹ Eye Clinic, Department of Biomedical and Clinical Science, Luigi Sacco Hospital, University of Milan, Milan, Italy.

² EBTNA-LAB, Rovereto (TN), Italy.

³ MAGI EUREGIO, Bolzano, Italy.

Disclosure(s):

All authors have completed and submitted the ICMJE disclosures form.

The author(s) have made the following disclosure(s): M.C.: Financial support – Bayer, Nide.

G.S.: Consultant – Heidelberg Engineering, Optos, OptoVue, CenterVue, Allergan, Bayer, Genetech, Novartis, Quantel Medical, Carl Zeiss Meditec, Bohringer, Topcon, Roche.

HUMAN SUBJECTS: Human subjects were included in this study. The human ethics committees at Luigi Sacco Hospital approved the study. All research adhered to the tenets of the Declaration of Helsinki. All participants provided informed consent.

No animal subjects were included in this study.

Author Contributions:

Conception and design: Romano, Airaldi, Cozzi, Oldani, Riva, Bertoni, Dautaj, Bertelli, Staurengi, Salvetti

Analysis and interpretation: Romano, Airaldi, Cozzi, Oldani, Riva, Bertoni, Dautaj, Bertelli, Staurengi, Salvetti

Data collection: Romano, Airaldi, Cozzi, Oldani, Riva, Bertoni, Dautaj, Bertelli, Staurengi, Salvetti

Obtained funding: Study was performed as part of regular employment duty at the Eye Clinic, Department of Biomedical and Clinical Science, Luigi Sacco Hospital, University of Milan, Milan, Italy. No additional funding was provided.

Overall responsibility: Romano, Airaldi, Cozzi, Oldani, Riva, Bertoni, Dautaj, Bertelli, Staurengi, Salvetti

Abbreviations and Acronyms:

AMD = age-related macular degeneration; **BAF** = blue-light fundus autofluorescence; **BCVA** = best-corrected visual acuity; **CI** = circularity index; **EMAP** = extensive macular atrophy with pseudodrusen-like appearance; **ETDRS** = Early Treatment Diabetic Retinopathy Study; **RPE** = retinal pigment epithelium.

Keywords:

Progression of atrophy, EMAP, Extensive macular atrophy with pseudodrusen-like appearance, Multimodal imaging, Visual outcomes.

Correspondence:

Francesco Romano, MD, Eye Clinic, Department of Biomedical and Clinical Sciences, Luigi Sacco Hospital, University of Milan, Via G.B. Grassi, 74, 20157 Milan, Italy. E-mail: francesco.romano@unimi.it.

References

- Hamel CP, Meunier I, Arndt C, et al. Extensive macular atrophy with pseudodrusen-like appearance: a new clinical entity. *Am J Ophthalmol*. 2009;147:609–620.
- Douillard A, Picot MD, Delcourt C, et al. Dietary, environmental, and genetic risk factors of extensive macular atrophy with pseudodrusen, a severe bilateral atrophy of middle-aged patients. *Sci Rep*. 2018;8:6840.
- Douillard A, Picot MC, Delcourt C, et al. Clinical characteristics and risk factors of extensive macular atrophy with pseudodrusen: the EMAP Case-Control National Clinical Trial. *Ophthalmology*. 2016;123:1865–1873.
- Holz FG, Bindewald-Wittich A, Fleckenstein M, et al. Progression of geographic atrophy and impact of fundus autofluorescence patterns in age-related macular degeneration. *Am J Ophthalmol*. 2007;143:463–472.
- Holz FG, Steinberg JS, Gobel A, et al. Fundus autofluorescence imaging in dry AMD: 2014 Jules Gonin Lecture of the Retina Research Foundation. *Graefes Arch Clin Exp Ophthalmol*. 2015;253:7–16.
- Strauss RW, Ho A, Munoz B, et al. The natural history of the Progression of Atrophy Secondary to Stargardt Disease (ProgStar) studies: design and baseline characteristics: ProgStar report no. 1. *Ophthalmology*. 2016;123:817–828.
- Parodi MB, Iacono P, Campa C, et al. Fundus autofluorescence patterns in Best vitelliform macular dystrophy. *Am J Ophthalmol*. 2014;158(5):1086–1092.

8. Yung M, et al. Clinical applications of fundus autofluorescence in retinal disease. *Int J Retina Vitreous*. 2016; Apr 8;2:12. doi: 10.1186/s40942-016-0035-x. eCollection 2016.
9. Krebs I, Lois N, Forrester JV. Fundus autofluorescence. *Graefes Arch Clin Exp Ophthalmol*. 2011;52:249–255.
10. Smith RT, Bernstein PS, Curcio CA. Rethinking A2E. *Invest Ophthalmol Vis Sci*. 2013;54:5543.
11. Querques G, Blanco R, Puche N, et al. Extensive macular atrophy with pseudodrusen-like appearance. *Ophthalmology*. 2013;120:429.
12. Parodi MB, Querques G. Choroidal neovascularization associated with extensive macular atrophy with pseudodrusen. *Optom Vis Sci*. 2015;92:S51–S54.
13. Rajabian F, Arrigo A, Bordato A, et al. Optical coherence tomography angiography in extensive macular atrophy with pseudodrusen-like appearance. *Trans Vis Sci Technol*. 2020;9:2.
14. Bindewald A, Bird AC, Dandekar SS, et al. Classification of fundus autofluorescence patterns in early age-related macular disease. *Invest Ophthalmol Vis Sci*. 2005;46:3309–3314.
15. Guymer RH, Rosenfeld PJ, Curcio CA, et al. Incomplete retinal pigment epithelial and outer retinal atrophy in age-related macular degeneration: Classification of Atrophy Meeting report 4. *Ophthalmology*. 2020;127(3):394–409.
16. Fleckenstein M, Mitchell P, Freund KB, et al. The progression of geographic atrophy secondary to age-related macular degeneration. *Ophthalmology*. 2018;125:369–390.
17. Zweifel SA, Engelbert M, Laud K, et al. Outer retinal tubulation: a novel optical coherence tomography finding. *Arch Ophthalmol*. 2009;127:1596–1602.
18. Dolz-Marco R, Glover JP, Gal-Or O, et al. Choroidal and sub-retinal pigment epithelium caverns: multimodal imaging and correspondence with friedman lipid globules. *Ophthalmology*. 2018;125:1287–1301.
19. Rahman W, Chen FK, Yeoh J. Repeatability of manual sub-foveal choroidal thickness measurements in healthy subjects using the technique of enhanced depth imaging optical coherence tomography. *Invest Ophthalmol Vis Sci*. 2011;52:2267–2271.
20. Domalpally A, Danis RP, White J, et al. Circularity index as a risk factor for progression of geographic atrophy. *Ophthalmology*. 2013;120:2666–2671.
21. Marsiglia M, Boddu S, Bearely S, et al. Association between geographic atrophy progression and reticular pseudodrusen in eyes with dry age-related macular degeneration. *Invest Ophthalmol Vis Sci*. 2013;54:7362–7369.
22. Kovach JL, Schwartz SG, Agarwal A, et al. The relationship between reticular pseudodrusen and severity of AMD. *Ophthalmology*. 2016;123:921–923.
23. Fleckenstein M, Schmitz-Valckenberg S, Martens C, et al. Fundus autofluorescence and spectral-domain optical coherence tomography characteristics in a rapidly progressing form of geographic atrophy. *Invest Ophthalmol Vis Sci*. 2011;52:3761–3766.
24. Batioglu F, Gedik Oguz Y, Demirel S, Ozmert E. Geographic atrophy progression in eyes with age-related macular degeneration: role of fundus autofluorescence patterns, fellow eye and baseline atrophy area. *Ophthalmic Res*. 2014;52:53–59.
25. Sunness JS, Margalit E, Srikumaran D, et al. The long-term natural history of geographic atrophy from age-related macular degeneration: enlargement of atrophy and implications for interventional clinical trials. *Ophthalmology*. 2007;114:271–277.
26. Gliem M, Muller PL, Birtel J, et al. Frequency, phenotypic characteristics and progression of atrophy associated with a diseased Bruch's membrane in pseudoxanthoma elasticum. *Invest Ophthalmol Vis Sci*. 2016;57:3323–3330.
27. Gliem M, Muller PL, Mangold E, et al. Sorsby fundus dystrophy: novel mutations, novel phenotypic characteristics, and treatment outcomes. *Invest Ophthalmol Vis Sci*. 2015;56:2664–2676.
28. Feuer WJ, Yehoshua Z, Gregori G, et al. Square root transformation of geographic atrophy area measurements to eliminate dependence of growth rates on baseline lesion measurements: a reanalysis of Age-Related Eye Disease Study report no. 26 [letter]. *JAMA Ophthalmol*. 2013;131:110–111.
29. Reiter GS, Told R, Baumann L, et al. Investigating a growth prediction model in advanced age-related macular degeneration with solitary geographic atrophy using quantitative autofluorescence. *Retina*. 2020;40:1657–1664.
30. Keenan TD, Agrón E, Domalpally A, et al. Progression of geographic atrophy in age-related macular degeneration: AREDS2 report number 16. *Ophthalmology*. 2018;125:1913–1928.
31. Zanzottera EC, Ach T, Huisingh C, et al. Visualizing retinal pigment epithelium phenotypes in the transition to geographic atrophy in age-related macular degeneration. *Retina*. 2016;36(Suppl 1):S12–S25.
32. Sarks S, Cherepanoff S, Killingsworth M, Sarks J. Relationship of basal laminar deposit and membranous debris to the clinical presentation of early age-related macular degeneration. *Invest Ophthalmol Vis Sci*. 2007;48:968–977.
33. Pellegrini M, Acquistapace A, Oldani M, et al. Dark atrophy: an optical coherence tomography angiography study. *Ophthalmology*. 2016;123:1879–1886.
34. Sacconi R, Corbelli E, Carnevali A, et al. Optical coherence tomography angiography in geographic atrophy. *Retina*. 2018;38:2350–2355.
35. Nattagh K, Zhou H, Rinella N, et al. OCT angiography to predict geographic atrophy progression using choriocapillaris flow void as a biomarker. *Transl Vis Sci Technol*. 2020;9:6.